Journal of Medicinal Chemistry

pubs.acs.org/jmc

Article

Balancing Affinity, Selectivity, and Cytotoxicity of Hydrazone-Based G-Quadruplex Ligands for Activation of Interferon β Genes in Cancer Cells

Simona Marzano, Giulia Miglietta, Rita Morigi,* Jessica Marinello, Andrea Arleo, Monica Procacci, Alessandra Locatelli, Alberto Leoni, Bruno Pagano, Antonio Randazzo, Jussara Amato,* and Giovanni Capranico*

Cite This: *J. Med. Chem.* 2022, 65, 12055−12067

Read Online

ACCESS | Metrics & More | Article Recommendations | Supporting Information

ABSTRACT: G-quadruplex (G4) ligands are investigated to discover new anticancer drugs with increased cell-killing potency. These ligands can induce genome instability and activate innate immune genes at non-cytotoxic doses, opening the discovery of cytostatic immune-stimulating ligands. However, the interplay of G4 affinity/selectivity with cytotoxicity and immune gene activation is not well-understood. We investigated a series of closely related hydrazone derivatives to define the molecular bases of immune-stimulation activity. Although they are closely related to each other, such derivatives differ in G4 affinity, cytotoxicity, genome instability, and immune gene activation. Our findings show that G4 affinity of ligands is a critical feature for immune gene activation, whereas a high cytotoxic potency interferes with it. The balance of G4 stabilization *versus* cytotoxicity can determine the level of immune gene activation in cancer cells. Thus, we propose a new rationale based on low cell-killing potency and high immune stimulation to discover effective anticancer G4 ligands.

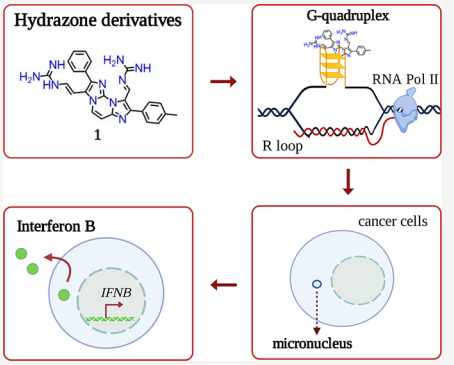

INTRODUCTION

G-quadruplex (G4) ligands are actively investigated to discover new effective anticancer drugs as G4s, non-canonical DNA structures, are considered promising targets.[1−4] Despite the large number of specific ligands developed, none has however shown efficacy in cancer patients and very few have reached early phases of clinical trials.[5,6] In line with the standard drug discovery rationale, several laboratories have previously searched for G4 binders with a high cell-killing potency.[1−5] Interestingly, we have recently demonstrated that the G4 binders pyridostatin (**PDS**) and PhenDC3 can effectively elicit an innate immune gene response [activation of interferon β (IFN-B) gene and IFN-B-dependent pathways] in human cancer cells, mediated by micronuclei accumulation at non-cytotoxic concentrations.[7] As recent advances clearly point to the potential of harnessing innate immunity for cancer immunotherapy,[8−12] non-cytotoxic immune-modulators may optimize immunotherapy in unresponsive cancers while having a marginal toxicity against proliferating normal cells. Thus, our recent findings[7] indicate that G4 ligands may be exploited as cytostatic immune-stimulating agents for anticancer immune-therapeutic combinations.[5] In particular, G4 binders can increase micronuclei,[7,13,14] which can be a source of cytoplasmic DNA that is able to induce the cGAS−STING pathway and activate innate immune genes.[7,15,16] However, the relationships among G4 affinity/selectivity, cell-killing potency, and genome instability determining a high level of immune gene activation by G4 ligands remains to be established.

Here, to answer this question, we have focused on a highly homogenous series of new compounds able to selectively target G4s. In 2010, some of us identified **FG** (Chart 1), a bis-guanylhydrazone derivative of diimidazo[1,2-*a*:1,2-*c*]-pyrimidine, as a potent and selective G4 stabilizer.[17] Then, we identified highly selective analogues with a preference for parallel G4 topology and ability to stabilize G4s in living cancer

Chart 1. Chemical Structures of the Lead Compounds FG and FIM (1 and 3 by Amato *et al.*,[18] respectively)

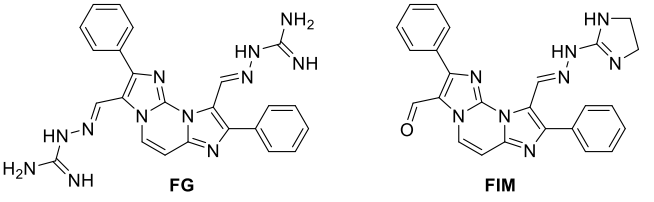

Received: May 16, 2022
Published: September 8, 2022

Chart 2. Chemical Structures of New FG and FIM Derivatives Synthesized in This Study

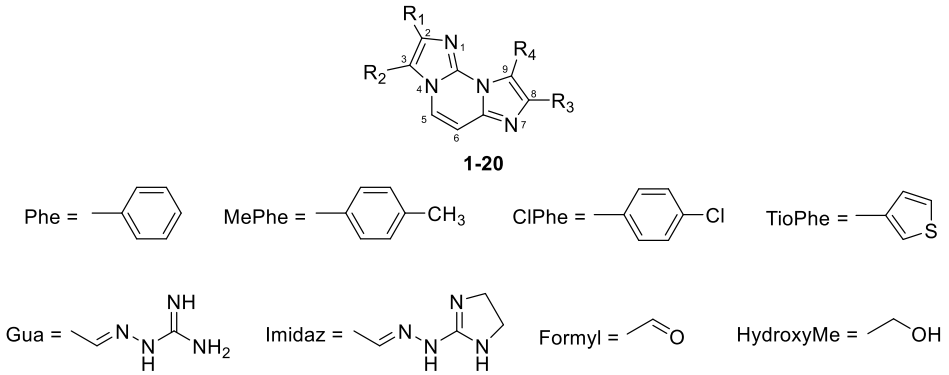

Comp	R_1	R_2	R_3	R_4
1	Phe	Gua	MePhe	Gua
2	Phe	Imidaz	MePhe	Imidaz
3	MePhe	Gua	Phe	Gua
4	MePhe	Imidaz	Phe	Imidaz
5	MePhe	Gua	MePhe	Gua
6	MePhe	Imidaz	MePhe	Imidaz
7	Phe	Gua	ClPhe	Gua
8	Phe	Imidaz	ClPhe	Imidaz
9	ClPhe	Gua	Phe	Gua
10	ClPhe	Imidaz	Phe	Imidaz
11	ClPhe	Gua	ClPhe	Gua
12	ClPhe	Imidaz	ClPhe	Imidaz
13	TioPhe	Imidaz	TioPhe	Imidaz
14	MePhe	Formyl	MePhe	Imidaz
15	Phe	Formyl	Phe	Gua
16	TioPhe	Formyl	TioPhe	Gua
17	MePhe	Formyl	Phe	Gua
18	MePhe	Formyl	MePhe	Gua
19	Phe	HydroxyMe	Phe	Imidaz
20	Phe	HydroxyMe	Phe	Gua

cells,[18] including **FG** and **FIM** (compounds **1** and **3** by Amato *et al.*,[18] respectively, Chart 1). The results established the diimidazo[1,2-*a*:1,2-*c*]pyrimidine core as a scaffold of selective G4 ligands and showed that both the iminoguanidine (Gua) and hydrazinoimidazoline (Imidaz) nitrogen chains are effective in achieving G4 binding properties. Then, **FG** was shown to induce DNA damage and micronuclei in human osteosarcoma U2OS cells in an R loop-dependent manner.[13]

As these agents are specific and effective G4 binders, we have now synthesized new close derivatives of **FG** and **FIM** to investigate the structural features eliciting a high immune gene activation relative to the cell-killing potency. The findings show that a proper balance between G4 affinity/selectivity and cytotoxicity is critical for immune gene activation in cancer cells.

RESULTS

Design of New Hydrazone-Based Compounds. In order to improve affinity and selectivity toward G4 structures and finely tune the biological effects of close **FG** and **FIM** analogues, we designed and synthesized a new series of molecules having different electron distribution and similar steric hindrance. For this purpose, the diimidazo[1,2-*a*:1,2-*c*]pyrimidine core was maintained unaltered and a chlorine or a methyl group was inserted at the para position of one or both the pending phenyl rings. In fact, chlorine and methyl have almost the same steric hindrance but opposite inductive effects, methyl being an electron donor group while chlorine has an electron withdrawing inductive effect. Both Gua and Imidaz moieties were considered as positively charged chains, either to obtain **FG** analogues (compounds **1**−**12**, Chart 2) or **FIM**

https://doi.org/10.1021/acs.jmedchem.2c00772
J. Med. Chem. 2022, 65, 12055−12067

Table 1. Compound-Induced Thermal Stabilization of G4 and haipin structures Measured by CD Melting Experiments

	$\Delta T_{1/2}$ (°C)[a]					
Comp	*tel*$_{26}$	*c-kit1*	*c-kit2*	*c-myc*	*hairpin*	no. of positive charges
FG[b]	−4.5	>15.0	>20	>20	0.1[c]	2
1	4.8 (±0.2)	18.2 (±0.2)	>30[d]	16.9 (±0.2)	1.3 (±0.3)	2
2	5.3 (±0.2)	15.2 (±0.2)	>30[d]	9.1 (±0.3)	1.1 (±0.4)	2
3	6.3 (±0.4)	25.2 (±0.5)	>30[d]	16.9 (±0.4)	3.2 (±0.3)	2
4	6.2 (±0.2)	21.4 (±0.4)	>30[d]	13.1 (±0.6)	2.2 (±0.2)	2
5	5.5 (±0.2)	18.5 (±0.3)	>30[d]	15.6 (±0.2)	4.1 (±0.3)	2
6	4.5 (±0.3)	17.1 (±0.2)	26.5 (±0.4)	8.5 (±0.2)	2.4 (±0.2)	2
7	5.0 (±0.2)	21.4 (±0.4)	>30[d]	17.6 (±0.4)	2.3 (±0.2)	2
8	6.3 (±0.2)	15.5 (±0.3)	22.0 (±0.3)	7.4 (±0.3)	1.2 (±0.4)	2
9	8.3 (±0.2)	20.1 (±0.3)	>30[d]	14.3 (±0.2)	2.6 (±0.2)	2
10	6.6 (±0.2)	17.7 (±0.3)	19.2 (±0.3)	10.6 (±0.3)	1.2 (±0.3)	2
11	4.1 (±0.4)	11.1 (±0.2)	>30[d]	11.4 (±0.2)	2.9 (±0.2)	2
12	3.3 (±0.2)	9.6 (±0.2)	13.7 (±0.3)	5.5 (±0.2)	3.5 (±0.2)	2
13	3.8 (±0.3)	10.3 (±0.2)	14.9 (±0.3)	4.7 (±0.2)	2.0 (±0.2)	2
FIM[b]	−3.0	2.7	9.5	>20	−0.8[c]	1
14	1.3 (±0.2)	3.8 (±0.2)	6.8 (±0.2)	1.5 (±0.2)	0.0 (±0.3)	1
15	4.3 (±0.2)	11.2 (±0.2)	24.2 (±0.4)	5.8 (±0.3)	1.7 (±0.2)	1
16	4.8 (±0.3)	16.1 (±0.2)	25.2 (±0.3)	9.1 (±0.3)	2.7 (±0.2)	1
17	3.8 (±0.2)	6.6 (±0.3)	20.8 (±0.5)	3.1 (±0.2)	1.2 (±0.2)	1
18	2.1 (±0.2)	6.1 (±0.2)	16.2 (±0.2)	4.6 (±0.2)	2.3 (±0.3)	1
19	2.0 (±0.2)	7.1 (±0.2)	14.7 (±0.3)	1.7 (±0.2)	1.3 (±0.2)	1
20	1.8 (±0.3)	9.7 (±0.2)	18.6 (±0.4)	2.8 (±0.2)	2.3 (±0.3)	1

[a]$\Delta T_{1/2}$ represents the difference in melting temperature [$\Delta T_{1/2} = T_{1/2}$ (DNA + 2 ligand equiv) − $T_{1/2}$ (DNA)]. The $T_{1/2}$ values of DNA alone are: *c-kit1* = 54.0 ± 0.5 °C, *c-kit2* = 61.5 ± 0.5 °C, *c-myc* = 72.0 ± 0.5 °C, *tel*$_{26}$ = 47.9 ± 0.5 °C, and *hairpin* = 75.4 ± 0.2 °C. All experiments were performed in duplicate, and the reported values are the average of two measurements. [b]Data from ref 18. [c]A self-complementary 12-mer duplex-forming sequence was used as a duplex model. [d]ΔT1/2 could not be accurately determined as the compound increases hugely the thermal stability of c-kit2.

analogues (compounds **14**−**18**, Chart 2). In addition, since an **FG** analogue bearing thiophenes instead of phenyl groups proved to be a good G4 binder,[18] we also considered this kind of modification along with the replacement of the Gua chains with the Imidaz ones (compound **13**, Chart 2). Finally, the formyl group of **FIM** was replaced with a primary alcohol group, which is able to either accept or donate hydrogen bonds (compounds **19** and **20**, Chart 2). The complete synthesis of the derivatives is described in Supporting Information (Scheme S1 and Table S1).

Circular Dichroism Experiments. The stabilizing effects of compounds **1**−**20** on G4 structures formed by the G-rich DNA sequences from the nuclease hypersensitive region of the c-KIT (*c-kit1* and *c-kit2*) and c-MYC (*c-myc*) gene promoters as well as from the human telomeric sequence (*tel*$_{26}$) were analyzed by circular dichroism (CD) melting experiments. These DNA sequences were chosen for their ability to adopt different G4 topologies, characterized by parallel (*c-kit1*, *c-kit2*, and *c-myc*) or hybrid (*tel*$_{26}$) arrangements.[19−21] Consistently, CD spectra of *c-kit1*, *c-kit2*, and *c-myc* displayed a positive band at 264 nm and a negative one around 240 nm (Figure S1), which are characteristics of parallel-stranded G4 topologies.[22] On the other hand, *tel*$_{26}$ showed a positive band at 290 with a shoulder at *ca.* 268 nm and a weak negative band at around 240 nm (Figure S1), confirming the presence of a hybrid structure as the main conformation. A 27 residue-long hairpin-forming oligonucleotide (*hairpin*) was also used to evaluate the selectivity of the new analogues for G4s over a duplex. CD spectra of *hairpin* showed a positive band at around 280 nm and a negative one at ∼250 nm, confirming the formation of a duplex (Figure S1). Additional CD spectra were recorded to examine the potential of compounds **1**−**20** to modify the native folding topology of these G4s. DNA/ligand mixtures were prepared by adding each ligand (2 molar equiv) to folded G4 or hairpin structures. No significant variations in the CD signal were observed for any of the analyzed DNA structures (Figures S2−S6), suggesting no G4 topology changes upon addition of compounds. Then, their ability to bind and stabilize the DNA structures was evaluated by CD melting experiments measuring the compound-induced change in the apparent melting temperature ($\Delta T_{1/2}$) of G4 and duplex structures. CD melting curves of DNA with and without each ligand were obtained by following the variations of the intensity of the CD signals at 264, 290, and 252 nm for parallel G4s, hybrid G4, and duplex, respectively (Figures S7−S11). The results show that all compounds are good G4 stabilizers (with one exception, **14**) showing a higher preference for parallel than hybrid G4s (Table 1). In addition, as expected for ligands having the same core but different numbers of positive charges, the greater the charge number, the stronger the stabilizing effect on G4s (Table 1). However, compound interactions with dsDNA (*hairpin*) were also slightly increased by positive charges (Table 1). Thus, to assess the selectivity for G4 structures of this series of compounds, we selected the analogues showing a strong stabilizing effect on at least two G4s and a negligible effect ($\Delta T_{1/2}$ < 2.0 °C) on the *hairpin*, that is, compounds **1**, **2**, **8**, and **10** among those with two positively charged side chains and **15**, **19**, and **20** among those with a positive charge only.

FRET Melting Experiments. The Förster resonance energy transfer (FRET) methodology[23] was used to further evaluate G4-stabilizing properties and G4 *versus* duplex

https://doi.org/10.1021/acs.jmedchem.2c00772
J. Med. Chem. 2022, 65, 12055−12067

selectivity of **1**, **2**, **8**, **10**, **15**, **19**, and **20**. In this assay, the G4-forming *c-kit1* oligonucleotide labeled with FAM (F) and TAMRA (T) at the 5′ and 3′ ends, respectively, was employed (*F-c-kit1-T*) since, among the G4s more stabilized by these ligands, *c-kit1* is the one that has the lowest $T_{1/2}$ value, thus allowing to better estimate the stabilizing properties of different ligands and evaluate their ability to discriminate between G4 and duplex structures. Indeed, as the target G4 was the only labeled molecule, it was possible to evaluate the ligand selectivity by adding a large excess of the *hairpin* oligonucleotide (unlabeled competitor). Therefore, the ability of the investigated compounds to selectively stabilize the G4 was evaluated by measuring the effect of the presence of various concentrations of the competitor on the $\Delta T_{1/2}$ of the G4 in the presence of 2 molar equiv of each ligand. Results of these experiments (Figure S12 and Table 2) confirm that the

Table 2. G4 Selectivity of the Selected Compounds[a]

	$\Delta T_{1/2}$ (°C)[b]		
Comp	*F-c-kit1-T*	*F-c-kit1-T* + *hairpin* (1:15)	*F-ckit1-T* + *hairpin* (1:50)
1	25.4 (±0.5)	22.2 (±0.5)	19.2 (±0.5)
2	22.4 (±0.5)	21.4 (±0.5)	20.2 (±0.5)
8	24.6 (±0.5)	21.4 (±0.5)	19.6 (±0.5)
10	26.6 (±0.5)	24.8 (±0.5)	23.8 (±0.5)
15	22.0 (±1.0)	21.6 (±1.0)	22.2 (±1.0)
19	8.0 (±0.4)	7.8 (±0.4)	8.4 (±0.4)
20	10.0 (±0.4)	11.1 (±0.5)	12.1 (±0.5)

[a]G4/dsDNA competition determined by ligand-induced thermal stabilization of *F-c-kit1-T* G4 measured by FRET. $\Delta T_{1/2}$ values are the differences between the $T_{1/2}$ of *F-c-kit1-T* in the presence (2 molar equiv) and absence of the ligands, without or with large excess of unlabeled *hairpin* (15 and 50 molar equiv with respect to G4). [b]The $T_{1/2}$ of *F-ckit1-T* is 57.4 (±0.2) °C. All experiments were performed at least in duplicate, and the reported values are the average of the measurements. The differences between results of CD and FRET melting experiments could be explained with different DNA sequences and/or experimental conditions.

selected compounds are efficient G4 stabilizers. However, in the case of compounds **1**, **2**, **8**, and **10** (carrying two positively charged side chains), G4/ligand interaction turned out to be somewhat challenged by the *hairpin* sequence being added in excess. This does not happen for **15**, **19**, and **20**, meaning that these compounds are more selective for G4 than the former.

Fluorescence Intercalator Displacement Assay. To gain insight into the affinity of the selected compounds for G4s, fluorescence intercalator displacement (G4-FID) experiments were performed by using the light-up fluorescent probe thiazole orange (TO), which binds to the DNA structure of interest.[24] The competitive displacement of TO from DNA by candidate ligands was monitored, thus enabling the determination of their relative binding affinity to the structures under examination, namely, *c-kit1*, *c-kit2*, and *c-myc* G4s, which were selected as they turned out to be those most stabilized by the ligands. Dose−response curves were obtained by plotting the percentage of TO displacement versus the concentration of each compound (Figure S13), and the concentrations at which 50% displacement was achieved (DC_{50}) were calculated. The lower the DC_{50} value, the higher should be the affinity of the compound for the DNA structure. Results of G4-FID assay (Table 3) indicate a good TO displacement ability for compounds **1**, **2**, **8**, and **10**. These ligands exhibited almost

Table 3. Ligand DC_{50} Values for *c-kit1*, *c-kit2*, and *c-myc* G4s Determined with G4-FID Assay

	DC_{50} (μM)[a]		
Comp	*c-kit1*	*c-kit2*	*c-myc*
1	1.4	1.4	1.6
2	1.3	1.2	1.3
8	2.7	1.7	1.8
10	1.2	1.4	1.3

[a]The error in DC_{50} values is ±5%.

similar results for the investigated parallel G4s, suggesting that ligand/G4 interaction is not sequence-specific. On the other hand, compounds **15**, **19**, and **20** were not able to reach 50% displacement in any case, suggesting that **FIM** derivatives have a lower affinity for G4s than **FG** ones. Therefore, the TO-displacing ability seems to be in direct correlation with the number of positive charges on the ligands: the highly cationic molecules are the most efficient TO displacers. As for **15**, the apparent discrepancy between the results of G4-FID assay and melting experiments (CD and FRET) could also be explained considering that this ligand may bind to G4s without strictly competing with the TO.[25]

Microscale Thermophoresis Assay. Quantitative data on the binding affinity of **1**, **2**, **8**, **10**, **15**, **19**, and **20** for the selected G4s were obtained by microscale thermophoresis (MST), which is a powerful method for the quantitative analysis of the interactions between small molecules and nucleic acids in solution.[26] To perform MST experiments, one of the binding partners must be fluorescent (either intrinsically fluorescent or conjugated to a given fluorophore). Therefore, serial dilutions of ligands were prepared, mixed with a constant concentration of Cy5.5-labeled G4s (*c-kit1*, *c-kit2*, and *c-myc*), and analyzed by MST. Results of the binding curves showed that the compounds bind to G4s with different affinity (Table 4 and Figures S14−S16). In particular, compounds showed

Table 4. Equilibrium Dissociation Constants for the Binding of the Ligands to *c-kit1*, *c-kit2*, and *c-myc* G4s Obtained by MST Experiments[a]

	K_d (μM)		
Comp	*c-kit1*	*c-kit2*	*c-myc*
1	0.03 ± 0.01	0.04 ± 0.01	1.5 ± 0.4
2	0.12 ± 0.02	0.13 ± 0.02	n.d.
8	0.38 ± 0.09	0.49 ± 0.09	3.0 ± 1.0
10	0.07 ± 0.02	0.50 ± 0.04	1.2 ± 0.4
15	0.30 ± 0.04	0.37 ± 0.03	7.0 ± 1.0
19	8.0 ± 2.0	2.5 ± 0.3	37 ± 1
20	2.0 ± 0.2	1.3 ± 0.2	8.0 ± 3.1

[a]Dissociation constant values were obtained with MST experiments. Comp, compound. n.d., not determined.

higher affinity values for *c-kit1* and *c-kit2* than for *c-myc*, and a slight preference for *c-kit1* over *c-kit2*, except for **19** and **20**. Noteworthy, compound **1** turned out to be the strongest G4 binder of the series, showing K_d values in the nanomolar range for the interaction with *c-kit1* and *c-kit2* [K_d = 0.03 and 0.04 μM, respectively], while **19** and **20** turned out to be the worst of the series in terms of affinity for G4s.

Cytotoxicity of Selected Hydrazone Derivatives. Next, we determined the cytotoxic potencies of compounds with two (**FG**, **1**, **2**, and **8**) or one (**FIM**, **15**, **19**, and **20**) positively

https://doi.org/10.1021/acs.jmedchem.2c00772
J. Med. Chem. 2022, 65, 12055−12067

charged chain in human osteosarcoma U2OS and murine fibrosarcoma MNMCA1 cells following 24 h of treatments by using **PDS** as a reference compound (Table 5). We selected these two lines as the former has been used in several G4 studies, included ours,[13,14,18] and the latter murine line is known to produce high levels of IFN-B.[27] The results show that **FIM** and **15**, both bearing an aldehyde moiety, are the most cytotoxic compounds among those analyzed (Table 5). In particular, they exhibited IC_{50} values around 6-fold and 5−18-fold higher than those of **19** and **20**, respectively, indicating that an aldehyde moiety confers a greater cytotoxicity than an alcohol group. Among the **FG** analogues, **8** is more cytotoxic than **1** and **2**. The compounds have similar IC_{50} in both the two lines; however, imino-guanidine chains confer around twofold higher cytotoxic activity than 2-hydrazino-2-imidazoline chains in humans but not in murine cells (compare **1** *vs* **2**, and **20** *vs* **19**, Table 5). To better define the interplay among G4 affinity/selectivity, G4 stabilization in cells, induction of genome instability and activation of IFN-B, **FG** and **FIM** analogues were discussed separately. The tested analogues show similar cytotoxic potency in normal human MRC5 fibroblasts (Table S2) as expected for a cell assay which measures cell-killing effects against proliferative cells.

Table 5. Cytotoxic Potency of Selected Hydrazone Derivatives[a]

Comp	human U2OS	murine MNMCA1
FG	15.9 ± 1.2[b]	n.d.
1	46.8 ± 12.7	38.5 ± 5.8
2	108.3 ± 35.4	28.6 ± 8.4
8	20.2 ± 1.0	23.5 ± 5.1
FIM	4.0 ± 0.33	2.3 ± 0.92
15	2.6 ± 0.87	1.9 ± 0.33
19	24.5 ± 1.2	12.1 ± 2.5
20	14.3 ± 9.3	35.7 ± 0.67
PDS	>50[b]	27.0 ± 16.0

[a]Data are IC_{50} (μM, concentration inhibiting 50% of cell growth) of each compound in human osteosarcoma U2OS cells and murine fibrosarcoma MNMCA1 cells. Treatments were for 24 h in exponentially growing cells. Cell survival was evaluated with the MTT test after 48 h of cell recovery in drug-free medium. IC_{50} values are means ± SEM of two independent experiments performed in triplicate. [b]See ref 13. n.d., not determined.

G4 Stabilization and DNA Damage by Hydrazone Derivatives with Two Side Chains. Next, we have evaluated cellular effects of closely related analogues starting with compounds **1**, **2**, and **8**, which have two positively charged side chains (Figure 1). We used an immunofluorescence (IF) assay to determine their ability to stabilize G4 structures in U2OS cells using the BG4 antibody, which specifically binds to G4 structures,[13,28] and **PDS** as the positive control.[13] The results (Figure 1A) show that **1** and **2** can stabilize G4 structures (around 2.4-fold increase) in living cells whereas compound **8** was ineffective (0.77-fold change). Analogues **1** and **2** showed a G4 stabilization *in vivo* similar to that of **PDS** (Figure 1A) and much higher than that of **8**, suggesting that the latter has other or additional cytotoxic mechanisms. Overall, these results agree with a higher ligand-induced G4 thermal stabilization observed for analogues **1** and **2** than that for **8**, particularly for *c-kit2* and *c-myc* G4s (Tables 1 and 3). The complete lack of G4 stabilization with **8** in nuclei suggests that G4 binding in living cells may be affected by interactions with other cellular components.

Next, we determined DNA damage induced by **1**, **2**, and **8** by evaluating the levels of S139-phosphorylated histone H2AX (γH2AX) (Figure 1B). We treated U2OS cancer cells with compounds for 24 h, at equal cytotoxic concentrations. **PDS** (10 μM) was used a reference compound.[13] The results show that **2** and **8** increased γH2AX foci levels (1.45- and 1.37-fold increase, respectively) whereas **1** did not. Thus, as **8** can induce DNA damage (Figure 1B) even without stabilizing G4s in cell (Figure 1A), while compound **2** induces G4 stabilization, it is reasonable to speculate that the cytotoxicity mechanism is likely different between the two compounds. On the other hand, G4 stabilization may lead to different levels of DNA damage, likely depending on *in vivo* G4 targeting. In contrast to **2**, compound **1** stabilizes G4 structures in cells (Figure 1A) but does not promote DNA damage (Figure 1B).

Micronuclei and IFN-B Activation by Hydrazone Derivatives with Two Side Chains. As non-cytotoxic doses of G4 binders, **PDS** and PhenDC3, can activate IFN-B-dependent pathways through micronuclei induction in human cancer cells,[7] we next ask if the new analogues can also affect immune gene expression in cancer cells. First, we determined the induction of micronuclei. **1**, **2**, and **8** at similar cytotoxic concentrations (15 μM, corresponding to 0.4−0.65 of their IC_{50}s) can induce almost the same micronuclei levels in MNMCA1 cells but less than those of **PDS** (Figure 1C). Then, we measured the amount of IFN-B secreted by murine MNMCA1 cells into the medium with ELISA assay. In agreement with experimental conditions reported for **PDS** previously,[7] murine cells were treated for 24 h with two concentrations (15 and 30 μM) of compounds and then allowed to recover for 2 days in fresh medium (Figure 1D). The results show that **PDS** induced higher IFN-B levels than the tested analogues, consistently with higher numbers of **PDS**-stimulated micronuclei. Among the studied analogues, **1** was more effective in the induction of IFN-B than **2**, whereas **8** was completely ineffective (Figure 1D). In particular, **1** induced IFN-B production at higher levels at non-cytotoxic concentrations (15 μM) and **8** was ineffective even at concentrations higher (30 μM) than the IC_{50} (Figure 1D and Table 5). Thus, compound **1**, which induces *in vivo* G4 stabilization without promoting DNA damage, can activate IFN-B gene expression at non-cytotoxic concentrations.

G4 Stabilization and DNA Damage by Hydrazone Derivatives with One Side Chain. Next, we have evaluated cellular effects of closely related analogues with one positively charged side chain, **FIM**, **15**, **19**, and **20**. Although these analogues showed a markedly decreased affinity for the tested G4 structures with respect to two positively charged analogues (Tables 1−3), their cytotoxic potencies are equal or higher than those of the latter (Table 5). Therefore, we asked whether **FIM** analogues could trigger G4 stabilization and DNA damage similar to **FG** analogues. The results show that they are all good G4 stabilizers in living cells (Figure 2A). **15** and **20** induced a somewhat higher stabilization (2.32−2.45-fold change) than **FIM** and **19** (1.55−1.91-fold change), indicating that the Gua moiety favors G4−ligand interactions better than the 2-hydrazino-2-imidazoline group (see also Table 1) probably due to its higher flexibility. Then, we investigated the ability of these analogues to induce DNA damage under the experimental conditions described above for **FG** analogues. The results show that these analogues increased γH2AX levels

https://doi.org/10.1021/acs.jmedchem.2c00772
J. Med. Chem. 2022, 65, 12055−12067

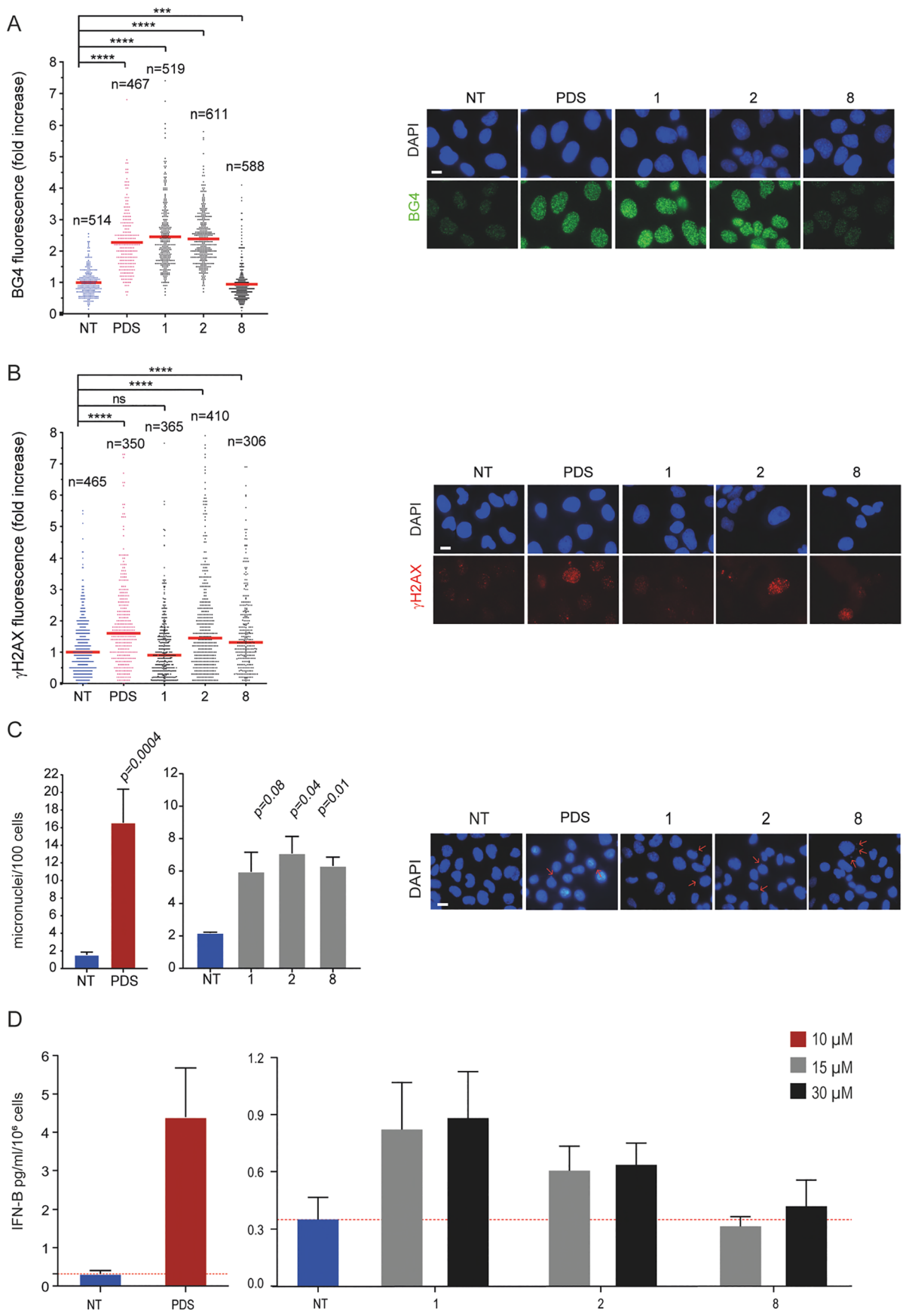

Figure 1. G4 stabilization, DNA damage, and IFN-B stimulation induced by **FG** derivatives. (A) Quantification of fluorescence signals of BG4 foci in U2OS cells being treated for 10 min with **PDS** or **FG** derivatives (compounds **1**, **2**, and **8**) at 10 μM concentration. The graph shows the fold increase reported as the mean ± SEM of three biological replicates, and the IF representative images are reported (left). (B) Quantification of

https://doi.org/10.1021/acs.jmedchem.2c00772
J. Med. Chem. 2022, 65, 12055−12067

Figure 1. continued

fluorescence signals of γH2AX in U2OS cells being treated with **PDS** (10 μM) and **FG** derivatives at IC_{50} concentrations (46, 100, and 20 μM for **1**, **2**, and **8**, respectively) for 24 h of treatment. The graph shows the fold increase reported as the median ± SEM of two biological replicates and the IF representative images are reported (left). (C) Micronuclei quantification by DAPI staining in MNMCA1 cells treated (15 μM) after 24 h of treatment followed by 24 h of drug-free recovery. **PDS** (10 μM)-treated cells are also shown. The graph shows the mean ± SEM of two biological replicates, and the IF representative images are reported (left). Above the bar chart, the *p*-value are reported. The scale bar is 10 μm. (D) Quantification of IFN-B produced by MNMCA1 cells treated with **FG** derivatives at different concentrations (15 and 30 μM). **PDS** (10 μM)-treated cells are also shown. The IFN-B detection was performed with ELISA assay after 24 h of compounds treatment followed by 48 h of recovery. The bar chart reports the mean ± SEM of three biological replicates. Significance in all the graph was calculated by Mann−Witney test (*$p < 0.05$, **$p > 0.01$, ***$p > 0.001$, and ****$p < 0.0001$).

at similar levels in cancer cells, even though **15** was somewhat less effective (Figure 2B). As **FIM** and **15** were more cytotoxic than **19** and **20**, DNA damage features of the former are likely more lethal than those of the latter.

Micronuclei and IFN-B Activation by Hydrazone Derivatives with One Side Chain. Similar to **FG** analogues (Figure 1), we then tested the **FIM** analogues for the induction of micronuclei and the activation of IFN-B genes in murine MNMCA1 cells by using sub-cytotoxic concentrations (Figure 2C,D). The results show that **FIM**, **15**, **19**, and **20** induced a 2.5−4.0-fold increase in micronuclei levels in comparison to untreated cells with little difference among them (Figure 2C). Overall, the **FIM** analogues did not affect significantly IFN-B expression, showing a low, if any, with a maximum of less than twofold change for **FIM** (Figure 2D). No difference was observed between derivatives bearing Gua or 2-hydrazino-2-imidazoline groups as chains. Overall, the results indicate that analogues with one positively charged side chain were less effective in activating the IFN-B gene expression than the two positively charged analogues (Figure 1). The effect on gene expression was thus correlated with G4 affinity of the studied analogues.

DISCUSSION

Hydrazone-based compounds, including **FG** and **FIM** (Chart 1), are known to have a high selectivity for G4 structures relative to duplex DNA and to induce DNA damage and genome instability.[14,17,18] Here, we provide evidence that these agents can activate IFN-B gene expression in cancer cells at non-cytotoxic doses, therefore pointing to the exploitation of hydrazone-based G4 ligands as immunomodulating agents. In particular, **1** can be considered as a core structure for further analyses aiming at establishing a hit ligand with immune-stimulating anticancer activity.

In vivo G4 selectivity of structurally different G4 ligands is substantially unknown as the number and types of G4 structures in a living cell can be very high.[3−5] In addition, a ligand can have more molecular interactions affecting its biological outcome, in particular the cell-killing potency. Thus, our present investigation has been focused on very closely related analogues to minimize putative variations of unpredictable molecular interactions. In particular, a new series of **FG** and **FIM** having different electron distribution and similar steric hindrance were designed and synthesized. For this purpose, the diimidazo[1,2-*a*:1,2-*c*]pyrimidine core was maintained unaltered and a chlorine or a methyl group was inserted at the para-position of one or both the pending phenyl rings. In fact, chlorine and methyl have almost the same steric hindrance but opposite inductive effects, methyl being an electron donor group while chlorine has an electron-withdrawing inductive effect. Both Gua and Imidaz moieties were considered as positively charged chains, either to obtain **FG** analogues (compounds **1**−**12**, Chart 2) or **FIM** analogues (compounds **14**−**18**). In addition, since an **FG** analogue bearing thiophenes instead of the phenyl groups proved to be a good G4 binder,[14] we also considered this kind of modification along with the replacement of the Gua chains with Imidaz ones (compound **13**). Finally, the formyl group of **FIM** was replaced with a primary alcohol group, which is able to either accept or donate hydrogen bonds (compounds **19** and **20**).

The G4 binding properties of **1**−**20** in terms of either G4 stabilization, affinity, and selectivity over the duplex structure were measured by means of several biophysical techniques, including CD, G4-FID, MST, and competition FRET-melting. We used the results of CD melting experiments to select the best binders from **FG** and **FIM** series. In particular, the ligands were chosen on the basis of their selectivity for G4 over the duplex, that is, those compounds showing the most negligible effects on the hairpin−duplex model (compounds **1**, **2**, **8**, and **10** belonging to the **FG** series; **15** and **17** belonging to the **FIM** series and exhibiting the formyl group; and **19** and **20** in which the formyl group of **FIM** is reduced to the corresponding hydroxyl group). Next, among these compounds, we selected, within each series, those that showed the greatest stabilizing effects on at least two G4s and differed in the presence of Gua or Imidaz pendant groups, that is, compounds **1** and **2** as **FG** analogues (with Gua and Imidaz substituents, respectively), compound **15** among the **FIM** derivatives (with a formyl group in R_2 and a Gua substituent in R_4), and compounds **19** and **20** among the hydroxyl group-containing **FIM** derivatives (carrying a Gua and an Imidaz pendant group in R_4, respectively). Since compounds **8** and **10** belonging to the **FG** series also showed good stabilizing properties on the investigated G4s, we decided to include them in further biophysical assays aimed at assessing the selectivity of the ligands (FRET) and their affinity for G4s (G4-FID assay).

The results of these studies confirmed that compounds **1**, **2**, **8**, **10**, and **15** are stronger G4 stabilizers than **19** and **20**, and revealed that compounds with one positively charged side chain (*i.e.*, **15**, **19**, and **20**) have less affinity for G4s but are more selective binders compared to those having two positively charged side chains (**1**, **2**, **8**, and **10**), with compounds **1**, **2**, and **10** being the most efficient TO displacers. Despite the high chemical similarity between **8** and **10** (they differ in the inversion of the Phe and ClPhe substituents in R_1 and R_3), only compound **10** performed similarly to **1** and **2**, while compound **8** showed a slightly lower G4 affinity. These results were also confirmed by MST experiments, which allowed to evaluate the affinity of the ligands for the G4s. Indeed, compound **1** turned out to be the

https://doi.org/10.1021/acs.jmedchem.2c00772
J. Med. Chem. 2022, 65, 12055−12067

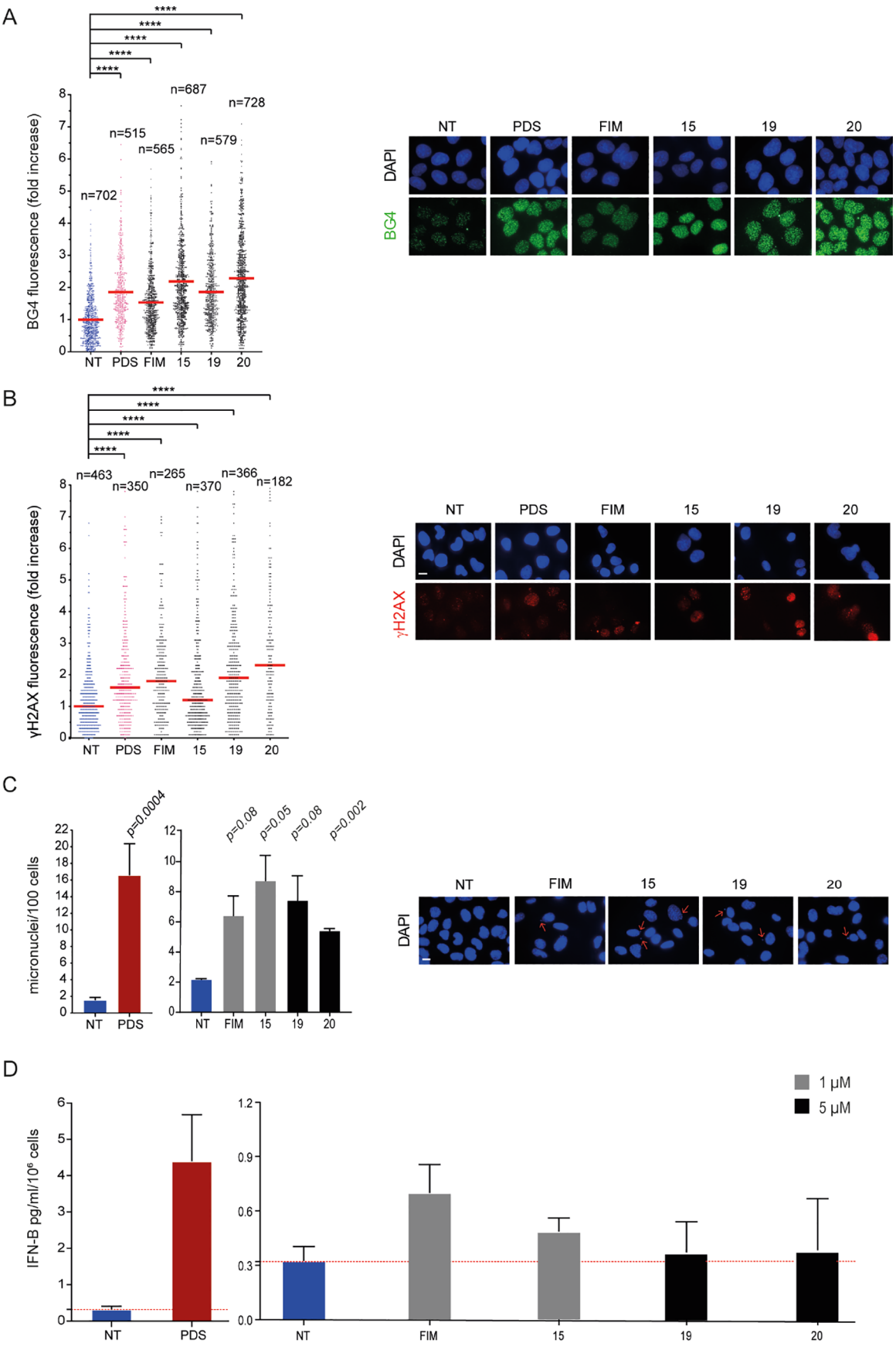

Figure 2. G4 stabilization, DNA damage, and IFN-B stimulation induced by **FIM** derivatives. (A) Quantification of fluorescence signals of BG4 foci in U2OS cells treated for 10 min with **PDS** or **FIM** derivatives at 10 μM concentration. Graphs show the fold increase reported as the mean ± SEM of three biological replicates. The images are representative of IF assays performed at reported concentrations (left). (B) Quantification of

https://doi.org/10.1021/acs.jmedchem.2c00772
J. Med. Chem. 2022, 65, 12055−12067

Figure 2. continued

fluorescence signals of γH2AX in U2OS cells treated with **PDS** (10 μM) and **FIM** derivatives at IC_{50} concentrations (4, 2.5, 24, and 14 μM for **FIM**, **15**, **19**, and **20**, respectively). The graph shows the fold increase reported as the median ± SEM of two biological replicates, and the IF representative images are reported (left). (C) Micronuclei quantification by DAPI staining in MNMCA1 cells treated with 1 μM of compounds **FIM** and **15** and 5 μM for the analogues **19** and **20**. **PDS** (10 μM)-treated cells are also shown. Left, the graph shows the mean ± SEM of two biological replicates; right, representative cell images. The scale bar is 10 μm. Above the bar chart, the *p*-value are reported. (D) Quantification of IFN-B stimulated at the reported concentration has been detected after 24 h of treatment followed by 48 h of recovery. **PDS** (10 μM)-treated cells are also shown. The IFN-B protein levels were detected with ELISA assay. The bar chart reports the mean ± SEM of two biological replicates. Significance in all the graphs was calculated by Mann−Whitney test (*$p < 0.05$, **$p > 0.01$, ***$p > 0.001$, and ****$p < 0.0001$).

strongest G4 binder, followed by **2** and **10**, while **19** and **20** were the worst of the series.

Based on the whole set of biophysical data, the compounds were classified according to their affinity for G4s: strong binders in the case of **1**, **2**, and **10**; moderate binders for **8** and **15**; and modest binders for **19** and **20**.

Therefore, aimed at defining the interplay between G4 affinity, stabilization in cells, cytotoxicity, and immune-stimulation activity of these hydrazone-based compounds, derivatives **1**, **2**, **8**, **15**, **19**, and **20**, having different affinity for G4s, were selected for the biological investigations.

Interestingly, despite the minimal structural differences among the **FG** analogues **1**, **2** and **8**, they showed interesting differences in cytotoxic potency, in-cell G4 stabilization, and IFN-B gene activation. Compound **8** is more cytotoxic than **1** and **2** (Table 5); however, it minimally stabilizes G4 in nuclei (Figure 1A) and it does not trigger IFN-B production (Figure 1D). On the contrary, **1** shows a high G4 stabilization *in vivo* (Figure 1A) and the least cytotoxic potency in murine cells (Table 5), where it triggers a good activation of IFN-B genes (Figure 1D).

Conversely, **FIM** analogues bearing the chemically reactive aldehyde group (**FIM** and **15**) or the hydroxymethyl group (**19** and **20**) exhibit a greater cytotoxic potency than **FG** derivatives (Table 5), with compounds **FIM** and **15** being the most cytotoxic compounds of the series. In addition, they are able to stabilize G4 in cells (Figure 2A) but not able to trigger IFN-B activation. These data clearly show that a high cytotoxic ability interferes with the ability of a G4 ligand to activate the expression of IFN-B genes. Overall, **FG** analogues, characterized by two side chains, exhibit a markedly higher G4 affinity than that of **FIM** analogues (Tables 1 and 3), albeit with a reduction of G4 selectivity (Table 2). As **FIM** analogues overall do not activate IFN-B genes (Figure 2D), whereas the **FG** analogue **1** does (Figure 1D), we speculate that a high ligand affinity for G4 may be required for immune gene activation. **FG** and **FIM** analogues can stabilize G4s at similar levels in nuclear chromatin; however, we do not know whether G4 structures stabilized by each analogue are the same or not. Our data indicate that the specific pattern of stabilized G4s and, likely, the specific time and location may affect the molecular response to G4 ligand activity.

An important observation was that IFN-B activation was independent of the level of induced micronuclei (Figures 1 and 2, panels C and D), suggesting that cytosolic DNA from micronuclei was necessary but not sufficient for immune gene expression.[29,30] Even though the definition of the mechanism likely needs future investigations, however, the activation of other cytoplasmic signaling pathways may affect the recognition of micronuclei and activation of the STING pathway.[5,29,30] Autophagic processes are known to be activated by G4 binders[3,31,32] and can regulate the STING pathway through recycling micronuclei and DNA by forming autophagosomes.[33,34] Interestingly, autophagic gene pathways were not activated at high levels in MCF-7 cells treated with **PDS**, which can activate at very high levels the IFN-B gene and other genes stimulated by IFN-B.[7] Therefore, differences in autophagic pathway activation might explain differences in IFN-B production between analogue **1** and other studied derivatives.

CONCLUSIONS

Comparing very closely related G4 binders has allowed us to demonstrate that a proper balance between G4 affinity/selectivity and cytotoxicity is critical for immune gene activation, in particular a high G4 affinity and a relatively low cytotoxic potency are necessary for a G4 ligand to activate IFN-B genes in cancer cells (Figure 3). Thus, we propose a new rationale, based on low cell-killing potency and high G4 affinity, to discover effective anticancer G4 ligands with immune-stimulation activity.

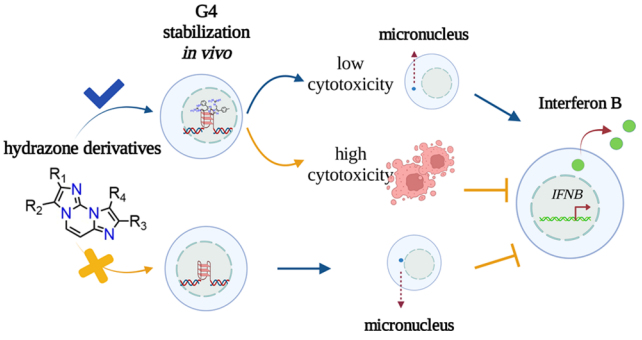

Figure 3. Schematic representation of cellular effects of hydrazone derivatives.

EXPERIMENTAL SECTION

Compound Synthesis and Materials. The synthesis and NMR spectra of **FG** and **FIM** analogues are reported in Supporting Information. All compounds are >95% pure by elemental analysis (see Supporting Information). Controlled pore glass supports, DNA phosphoramidites, all reagents for oligonucleotide synthesis and purification, and all other reagents and solvents were purchased from Merck KGaA (Darmstadt, Germany) and used without further purification. Dual-labeled FAM/TAMRA oligonucleotides and Cy5.5-labeled oligonucleotides were purchased from Biomers (Ulm, Germany).

Oligonucleotide Synthesis and Sample Preparation. The following deoxyribonucleotide sequences were used in this study: d(AGG GAG GGC GCT GGG AGG AGG G) (*c-kit1*), d(CGG GCG GGC GCT AGG GAG GGT) (*c-kit2*), d(TGA GGG TGG GTA GGG TGG GTA A) (*c-myc*), d(TTA GGG TTA GGG TTA GGG TTA GGG TT) (tel_{26}), and d(CGC GAA TTC GCG TTT CGC GAA TTC GCG) (*hairpin*). These oligonucleotides were chemically synthesized on the 1 μmol scale on an ABI 394 DNA/

https://doi.org/10.1021/acs.jmedchem.2c00772
J. Med. Chem. 2022, 65, 12055−12067

RNA synthesizer (Applied Biosystems, CA, USA) by using the standard β-cyanoethyl phosphoramidite solid-phase chemistry, as described elsewhere.[35] After synthesis, oligonucleotides were detached from the support and deprotected by treating with an aqueous solution of concentrated ammonia at 55 °C, for 17 h. The filtrates and washings, after being combined and concentrated under reduced pressure, were solubilized in water and purified using a high-performance liquid chromatography system equipped with a Nucleogel SAX column (Macherey-Nagel, 1000-8/46), using a 30 min linear gradient from 100% buffer A to 100% buffer B at a flow rate of 1 mL/min, with buffer A consisting of a 20 mM KH_2PO_4/K_2HPO_4 aqueous solution (pH 7.0) and buffer B consisting of 1.0 M KCl and 20 mM KH_2PO_4/K_2HPO_4 aqueous solution (pH 7.0). Both buffer A and B also contained 20% (v/v) CH_3CN. The purified fractions were then desalted by means of C-18 cartridges (Sep-Pak). The purity of the isolated oligomers was checked by NMR and proved to be higher than 98%. All oligonucleotides were dissolved in a buffer solution consisting of 5 mM KH_2PO_4/K_2HPO_4 (pH 7.0) and 20 mM KCl (or LiCl in the case of *c-myc* because of its high thermal stability). The concentration of each oligonucleotide was verified by measuring the UV absorption at 90 °C, considering the appropriate molar extinction coefficient values ε (λ = 260 nm) calculated using the nearest-neighbor model.[36] Finally, to achieve the correct folding of the DNA sequences, oligonucleotide solutions were annealed by heating at 95 °C for 5 min followed by a slow cooling to room temperature and storage overnight at 4 °C.

CD Experiments. CD experiments were performed on a Jasco J-815 spectropolarimeter equipped with a PTC-423S/15 Peltier temperature controller. All the spectra were recorded at 20 and 100 °C in the wavelength range of 230−320 nm and averaged over three scans. A scan rate of 100 nm/min, with a 0.5 s response time and 1 nm bandwidth, was used. The buffer baseline was subtracted from each spectrum. For the CD experiments, 10 μM G4 and 15 μM duplex DNA in the absence or presence of 2 molar equiv of ligand were used. CD spectra were recorded 10 min after ligand addition. Ligand stock solutions were 10 mM in DMSO. CD melting experiments were carried out in the 20−100 °C temperature range at a 1 °C/min heating rate by following the changes in the CD signal at the wavelengths of the maximum CD intensity (263 nm) for *c-kit1*, *c-kit2*, *c-myc*, and (287 nm) tel_{26} G4s, or minimum CD intensity (252 nm) for the *hairpin*. CD melting experiments were recorded both in the absence and presence of compounds (2 molar equiv) added to the folded nucleic acid structures. The apparent melting temperatures ($T_{1/2}$) were determined from a curve fit using OriginPro 2021 software (OriginLab Corp., MA, USA). $\Delta T_{1/2}$ values were determined as the difference in the $T_{1/2}$ values of the nucleic acid structures in the presence and absence of the compounds. Normalization of melting curves between 0 and 1 was performed to better compare the results. In cases where the melting process was not completed even at 100 °C due to an exceptional ligand-induced G4 thermal stabilization, the relative melting curves were normalized by dividing only by the maximum.

FRET Melting Experiments. Measurements were carried out on a Jasco FP-8300 spectrofluorometer equipped with a Peltier temperature controller system (PCT-818) using a dual-labeled G4-forming sequence FAM-[d(CGG GCG GGC GCT AGG GAG GGT)]-TAMRA (*F-c-kit1-T*). The oligonucleotide was dissolved in water at 1 mM, diluted at 1 μM using 5 mM KH_2PO_4/K_2HPO_4 (pH 7.0) containing 20 mM KCl, and annealed by heating to 90 °C for 5 min, followed by slow cooling to room temperature overnight and storage at 4 °C for 24 h before data acquisition. Experiments were performed in sealed quartz cuvettes with a path length of 1 cm by using 0.2 μM prefolded *F-c-kit1-T* target, in the absence and presence of 2 molar equiv of the ligand and of the *duplex* competitor at 3 and 10 μM final concentrations. In addition, an experiment in the absence of compounds and competitors was also performed. Fluorescence spectra were acquired before and after melting assay (15 and 90 °C, respectively). The dual-labeled oligonucleotide was excited at 492 nm, and emission spectra were recorded between 500 and 650 nm by using a 100 nm/s scan speed. Excitation and emission slit widths were both set to 5 nm. FRET melting experiments were performed by monitoring the emission of FAM at 520 nm (upon excitation at 492 nm), using a heating gradient of 0.2 °C/min over the range 15−90 °C. Emission of FAM was normalized between 0 and 1. Final analysis of the data was carried out using OriginPro 2021 software.

Fluorescent Intercalator Displacement (G4-FID) Assay. A solution containing 0.25 μM G4 DNA (*c-kit1*, *c-kit2*, or *c-myc*) and 0.5 μM TO in 5 mM KH_2PO_4/K_2HPO_4 buffer (pH 7.0) containing 20 mM KCl (or LiCl in the case of *c-myc*) was prepared in a 1 cm-path length cell, and the corresponding fluorescence spectrum was acquired in the absence and presence of increasing concentrations of selected compounds (1 mM stock solution in DMSO). Each ligand addition (from 0.5 to 20 molar equiv) was followed by a 3 min equilibration time before spectrum acquisition. Measurements were run at 20 °C on a Jasco FP-8300 spectrofluorometer equipped with a Peltier cell holder (PCT-818), using an excitation wavelength of 485 nm and recording the emission in the 500−650 nm wavelength range. Both excitation and emission slits were set at 5 nm. Final analysis of the data was carried out using OriginPro 2021 software. The percentage of TO displacement was calculated as follows: TO displacement (%) = $100 - [(F/F_0) \times 100]$, where F_0 is the fluorescence in the absence of a ligand and F is the fluorescence after each ligand addition. The percentage of displacement was then plotted as a function of the ligand concentration, and DC_{50} was calculated as the required concentration to displace 50% TO. Each titration was performed in duplicate.

Microscale Thermophoresis. MST measurements were performed using a Monolith NT.115 instrument (NanoTemper Technologies). The Cy5.5 fluorescently labeled oligonucleotides (*c-kit1*, *c-kit2*, and *c-myc*) were prepared at 1 μM in 5 mM KH_2PO_4/K_2HPO_4 buffer (pH 7.0) containing 20 mM KCl and annealed as described above. DNA samples were then diluted using the same phosphate buffer supplemented with 0.1% Tween. For the MST experiments, the concentration of the labeled oligonucleotides was kept constant at 20 nM, while a serial dilution of the ligand (1:2 from 5.0, 40, 160, or 400 μM ligand stock solution) in the same buffer used for DNAs was prepared and mixed with the oligonucleotide solution with a volume ratio of 1:1. All the samples, containing 20% DMSO as the final concentration, were loaded into standard capillaries (NanoTemper Technologies). Measurements were performed and analyzed as previously reported.[37]

Cell Lines and Treatments. Human osteosarcoma U2OS and murine fibrosarcoma MNMCA1 cell lines were grown in monolayer cultures in Dulbecco's modified Eagle medium (DMEM) supplemented with 10% fetal bovine serum (FBS) (Gibco) and 1% L-glutamine (Gibco). Human fibroblast lung MRC5 cells were grown in a monolayer culture in DMEM, supplemented with Ham's F-10 nutrient mix (1:1), 10% FBS, and Pen/Strep 100 μg/mL. All cell lines were grown in a humidified incubator at 37 °C and 5% of CO_2. Cell line identity was routinely checked by genotyping (BMR Genomics). Compounds were dissolved in dimethyl sulfoxide (Sigma-Aldrich #472301) at 10 mM concentration, stored in aliquots at −20 °C, and diluted to final concentrations immediately prior to use.

MTT Cell Proliferation Assay. U2OS, MNMCA1, and MRC5 cells (3×10^4) were seeded in 24 wells. 24 h after seeding, cells were treated with increasing concentrations of compounds for 24 h. Then, compounds were removed, and the cells were grown in complete drug-free medium for 48 h. Then, thiazolyl blue tetrazolium bromide (MTT) (Merck #2128) solution (0.45 μg/mL) was added to each well and incubated for 1 h at 37 °C. After incubation, the medium was removed and 300 μL of dimethyl sulfoxide was added and incubated for 1 h at room temperature. Then, 100 μL of the solution was put in 96 wells, and absorbance at 540 nm was measured using a multiplate reader. The linear regression parameters were determined to calculate the IC_{50} (GraphPad Prism 4.0, Graph Pad Software Inc.).

IF Microscopy. U2OS cells (3.5×10^5) were seeded in 35 mm dish on coverslips. The BG4 fluorescence signal was determined after 10 min of treatment at the reported concentrations. The BG4 antibody was purified as described.[13] Briefly, BG4 was isolated from *Escherichia coli* extracts by using silica-based resin (Thermo #89964)

https://doi.org/10.1021/acs.jmedchem.2c00772
J. Med. Chem. 2022, 65, 12055−12067

precharged with Co^{2+} ions and eluted with 250 μM imidazole/PBS pH 8.0. The eluted antibody was concentrated in Pierce 30k MWCO tubes (Pierce #88529), and imidazole was finally removed by buffer exchange with intracellular cell salt buffer in Pierce 30k MWCO tubes. For BG4 staining, cells were pre-fixed with cell culture medium and fix solution (1:1) and then incubated with the fix solution composed of methanol and acetic acid (3:1) for 10 min at RT. The cells were permeabilized with 0.1% of Triton X-100 in PBS and blocked in 2% non-fat milk for 1 h at RT under gentle shaking. Next, cells were stained with 0.5 μg of BG4 for 2 h at room temperature. Next, cells were incubated with the anti-FLAG antibody (dilution 1/800) (Cell Signaling Technology #2368) for 1 h and then stained with the Alexa Fluor 488 anti-rabbit IgG (Life technologies #A11008). For S139-phosphorylated histone H2AX, γH2AX cells were treated with compounds at the reported concentrations for 24 h. Then, cells were fixed with 4% formaldehyde for 10 min, permeabilized with 0.5% Triton X-100 in PBS for 15 , and then incubated with 8% BSA in PBS for 30 min at RT. Next, cells were stained with anti-γH2AX antibodies (#05-636, Millipore) diluted to 1:500 and next incubated for 1 h with Alexa Fluor 594 anti-mouse IgG (#A11032, Life Technologies). For DNA staining, cells were incubated with 2 μg/μL DAPI for 20 min. The cover glasses were mounted with Mowiol 488. The slides were visualized at room temperature by using a fluorescence microscope (Eclipse TE 2000-S, Nikon) equipped with an AxioCam MRm (Zeiss) digital camera. The fluorescence signal was quantified by using ImageJ software and reported as a fold increase of the non-treated sample. Graphs were prepared with GraphPad Prism 8.

IFN-B ELISA Assay. MNMCA1 cells (8×10^5) were seeded in a 10 mm dish. IFN-B protein levels were measured in cell medium supernatants. Culture medium of untreated and treated MNMCA1 cells was collected after 24 h of treatment followed by 48 h of drug recovery. Supernatants were added with protease inhibitors (1 mg/mL pepstatin, leupeptin, and aprotinin, 2 mM DTT, and 0.5 mM PMSF) and then concentrated around 25-fold by using a Pierce Protein Concentrator PES, 3k MWCO, 5−20 mL (#88525, Thermo Fisher). IFN-B protein levels were quantified with a human IFN-B Quantikine ELISA kit (MIFNB0, R&D Systems) following manufacturer's instructions. IFN-B levels were normalized over the cell number.

■ ASSOCIATED CONTENT

Supporting Information

The Supporting Information is available free of charge at https://pubs.acs.org/doi/10.1021/acs.jmedchem.2c00772.

Molecular formula strings (CSV)

Synthesis of compounds 1-20, NMR spectrometry characteristics, UHPLC system and conditions, and ^{1}H and ^{13}C spectra of compounds 1-20 (PDF)

■ AUTHOR INFORMATION

Corresponding Authors

Rita Morigi − *Department of Pharmacy and Biotechnology, Alma Mater Studiorum—University of Bologna, 40126 Bologna, Italy;* orcid.org/0000-0003-4739-8733; Phone: +39 051 2099725; Email: rita.morigi@unibo.it

Jussara Amato − *Department of Pharmacy, University of Naples Federico II, 80131 Naples, Italy;* orcid.org/0000-0001-6096-3544; Phone: +39 081 678630; Email: jussara.amato@unina.it

Giovanni Capranico − *Department of Pharmacy and Biotechnology, Alma Mater Studiorum—University of Bologna, 40126 Bologna, Italy;* orcid.org/0000-0002-8708-6454; Phone: +39 051 2091209; Email: giovanni.capranico@unibo.it

Authors

Simona Marzano − *Department of Pharmacy, University of Naples Federico II, 80131 Naples, Italy*

Giulia Miglietta − *Department of Pharmacy and Biotechnology, Alma Mater Studiorum—University of Bologna, 40126 Bologna, Italy*

Jessica Marinello − *Department of Pharmacy and Biotechnology, Alma Mater Studiorum—University of Bologna, 40126 Bologna, Italy*

Andrea Arleo − *Department of Pharmacy and Biotechnology, Alma Mater Studiorum—University of Bologna, 40126 Bologna, Italy;* orcid.org/0000-0002-3262-7268

Monica Procacci − *Department of Pharmacy and Biotechnology, Alma Mater Studiorum—University of Bologna, 40126 Bologna, Italy*

Alessandra Locatelli − *Department of Pharmacy and Biotechnology, Alma Mater Studiorum—University of Bologna, 40126 Bologna, Italy*

Alberto Leoni − *Department of Pharmacy and Biotechnology, Alma Mater Studiorum—University of Bologna, 40126 Bologna, Italy*

Bruno Pagano − *Department of Pharmacy, University of Naples Federico II, 80131 Naples, Italy;* orcid.org/0000-0002-7716-9010

Antonio Randazzo − *Department of Pharmacy, University of Naples Federico II, 80131 Naples, Italy;* orcid.org/0000-0002-9192-7586

Complete contact information is available at: https://pubs.acs.org/10.1021/acs.jmedchem.2c00772

Author Contributions

S.M., G.M., and R.M. contributed equally. R.M., A. Locatelli, and A. Leoni synthesized derivatives. S.M., B.P., and J.A. performed oligonucleotide synthesis and biophysical experiments. G.M., A.A., J.M., and M.P. performed the biological experiments. A.R., J.A., and G.C. designed, planned, and supervised experimental work and interpreted the results with all authors. The manuscript was written by G.C., J.A., G.M., and R.M. and with contributions from other authors. All authors approved the final version of the manuscript.

Notes

The authors declare no competing financial interest.

■ ACKNOWLEDGMENTS

We thank all laboratory members for helpful discussion. The research leading to these results had received funding from AIRC (Associazione Italiana per la Ricerca sul Cancro), IG 2019—ID 23032 project—PI G.C., IG 2020—ID 24590 project—PI B.P and IG 2021—ID 26313 project-PI A.R. G.M. is a recipient of a FIRC-AIRC postdoc fellowship from Italy [23953].

■ ABBREVIATIONS

BSA, bovine serum albumin; CBR, condensed benzene ring; CD, circular dichroism; DAPI, 4′,6-diamidino-2-phenylindole; DMEM, Dulbecco's modified Eagle medium; DMF, dimethylformamide; DSB, double-strand break; FAM, fluorescein; FBS, fetal bovine serum; FID, fluorescence intercalator displacement; FRET, Förster resonance energy transfer; G4, G-quadruplex; γH2AX, S139-phosphorylated histone H2AX; IF, immunofluorescence; IFN-B, interferon β; MST, microscale thermophoresis; NOE, nuclear overhauser effect; PBS,

https://doi.org/10.1021/acs.jmedchem.2c00772
J. Med. Chem. 2022, 65, 12055−12067

phosphate-buffered saline; **PDS**, pyridostatin; PIPES, 1,4-piperazinediethanesulfonic acid; TAMRA, carboxytetramethylrhodamine; TO, thiazole orange

REFERENCES

(1) Balasubramanian, S.; Hurley, L. H.; Neidle, S. Targeting G-Quadruplexes in Gene Promoters: A Novel Anticancer Strategy? *Nat. Rev. Drug Discovery* **2011**, *10*, 261−275.

(2) Neidle, S. Quadruplex Nucleic Acids as Novel Therapeutic Targets. *J. Med. Chem.* **2016**, *59*, 5987−6011.

(3) Carvalho, J.; Mergny, J.-L.; Salgado, G. F.; Queiroz, J. A.; Cruz, C. G-Quadruplex, Friend or Foe: The Role of the G-Quartet in Anticancer Strategies. *Trends Mol. Med.* **2020**, *26*, 848−861.

(4) Miglietta, G.; Russo, M.; Capranico, G. G-Quadruplex−R-Loop Interactions and the Mechanism of Anticancer G-Quadruplex Binders. *Nucleic Acids Res.* **2020**, *48*, 11942−11957.

(5) Miglietta, G.; Marinello, J.; Russo, M.; Capranico, G. Ligands Stimulating Antitumour Immunity as the next G-Quadruplex Challenge. *Mol. Cancer* **2022**, in press.

(6) Hilton, J.; Gelmon, K.; Bedard, P. L.; Tu, D.; Xu, H.; Tinker, A. V.; Goodwin, R.; Laurie, S. A.; Jonker, D.; Hansen, A. R.; Veitch, Z. W.; Renouf, D. J.; Hagerman, L.; Lui, H.; Chen, B.; Kellar, D.; Li, I.; Lee, S.-E.; Kono, T.; Cheng, B. Y. C.; Yap, D.; Lai, D.; Beatty, S.; Soong, J.; Pritchard, K. I.; Soria-Bretones, I.; Chen, E.; Feilotter, H.; Rushton, M.; Seymour, L.; Aparicio, S.; Cescon, D. W. Results of the Phase I CCTG IND.231 Trial of CX-5461 in Patients with Advanced Solid Tumors Enriched for DNA-Repair Deficiencies. *Nat. Commun.* **2022**, *13*, 3607.

(7) Miglietta, G.; Russo, M.; Duardo, R. C.; Capranico, G. G-Quadruplex Binders as Cytostatic Modulators of Innate Immune Genes in Cancer Cells. *Nucleic Acids Res.* **2021**, *49*, 6673−6686.

(8) Woo, S.-R.; Corrales, L.; Gajewski, T. F. Innate Immune Recognition of Cancer. *Annu. Rev. Immunol.* **2015**, *33*, 445.

(9) Poh, A. STINGing Antitumor Immunity into Action. *Cancer Discovery* **2018**, *8*, 259−260.

(10) Hartmann, G. Nucleic Acid Immunity. *Adv. Immunol.* **2017**, *133*, 121−169.

(11) van den Boorn, J. G.; Hartmann, G. Turning Tumors into Vaccines: Co-Opting the Innate Immune System. *Immunity* **2013**, *39*, 27−37.

(12) Fu, J.; Kanne, D. B.; Leong, M.; Glickman, L. H.; McWhirter, S. M.; Lemmens, E.; Mechette, K.; Leong, J. J.; Lauer, P.; Liu, W.; Sivick, K. E.; Zeng, Q.; Soares, K. C.; Zheng, L.; Portnoy, D. A.; Woodward, J. J.; Pardoll, D. M.; Dubensky, T. W.; Kim, Y. STING Agonist Formulated Cancer Vaccines Can Cure Established Tumors Resistant to PD-1 Blockade. *Sci. Transl. Med.* **2015**, *7*, 283ra52.

(13) De Magis, A.; Manzo, S. G.; Russo, M.; Marinello, J.; Morigi, R.; Sordet, O.; Capranico, G. DNA Damage and Genome Instability by G-Quadruplex Ligands Are Mediated by R Loops in Human Cancer Cells. *Proc. Natl. Acad. Sci. U.S.A.* **2019**, *116*, 816−825.

(14) Amato, J.; Miglietta, G.; Morigi, R.; Iaccarino, N.; Locatelli, A.; Leoni, A.; Novellino, E.; Pagano, B.; Capranico, G.; Randazzo, A. Monohydrazone Based G-Quadruplex Selective Ligands Induce DNA Damage and Genome Instability in Human Cancer Cells. *J. Med. Chem.* **2020**, *63*, 3090−3103.

(15) Harding, S. M.; Benci, J. L.; Irianto, J.; Discher, D. E.; Minn, A. J.; Greenberg, R. A. Mitotic Progression Following DNA Damage Enables Pattern Recognition within Micronuclei. *Nature* **2017**, *548*, 466−470.

(16) Mackenzie, K. J.; Carroll, P.; Martin, C.-A.; Murina, O.; Fluteau, A.; Simpson, D. J.; Olova, N.; Sutcliffe, H.; Rainger, J. K.; Leitch, A.; Osborn, R. T.; Wheeler, A. P.; Nowotny, M.; Gilbert, N.; Chandra, T.; Reijns, M. A. M.; Jackson, A. P. CGAS Surveillance of Micronuclei Links Genome Instability to Innate Immunity. *Nature* **2017**, *548*, 461−465.

(17) Sparapani, S.; Bellini, S.; Gunaratnam, M.; Haider, S. M.; Andreani, A.; Rambaldi, M.; Locatelli, A.; Morigi, R.; Granaiola, M.; Varoli, L.; Burnelli, S.; Leoni, A.; Neidle, S. Bis-Guanylhydrazone Diimidazo[1,2-a:1,2-c]Pyrimidine as a Novel and Specific G-Quadruplex Binding Motif. *Chem. Commun.* **2010**, *46*, 5680.

(18) Amato, J.; Morigi, R.; Pagano, B.; Pagano, A.; Ohnmacht, S.; De Magis, A.; Tiang, Y.-P. Y. P.; Capranico, G.; Locatelli, A.; Graziadio, A.; Leoni, A.; Rambaldi, M.; Novellino, E.; Neidle, S.; Randazzo, A. Toward the Development of Specific G-Quadruplex Binders: Synthesis, Biophysical, and Biological Studies of New Hydrazone Derivatives. *J. Med. Chem.* **2016**, *59*, 5706−5720.

(19) Hsu, S. T. D.; Varnai, P.; Bugaut, A.; Reszka, A. P.; Neidle, S.; Balasubramanian, S. A G-Rich Sequence within the c-Kit Oncogene Promoter Forms a Parallel G-Quadruplex Having Asymmetric G-Tetrad Dynamics. *J. Am. Chem. Soc.* **2009**, *131*, 13399−13409.

(20) Ambrus, A.; Chen, D.; Dai, J.; Jones, R. A.; Yang, D. Solution Structure of the Biologically Relevant G-Quadruplex Element in the Human c-MYC Promoter. Implications for G-Quadruplex Stabilization. *Biochemistry* **2005**, *44*, 2048−2058.

(21) Dai, J.; Carver, M.; Punchihewa, C.; Jones, R. A.; Yang, D. Structure of the Hybrid-2 Type Intramolecular Human Telomeric G-Quadruplex in K+ Solution: Insights into Structure Polymorphism of the Human Telomeric Sequence. *Nucleic Acids Res.* **2007**, *35*, 4927−4940.

(22) Randazzo, A.; Spada, G. P.; da Silva, M. W. Circular Dichroism of Quadruplex Structures. *Top. Curr. Chem.* **2013**, *330*, 67−86.

(23) Decian, A.; Guittat, L.; Kaiser, M.; Sacca, B.; Amrane, S.; Bourdoncle, A.; Alberti, P.; Teuladefichou, M. P.; Lacroix, L.; Mergny, J. L. Fluorescence-Based Melting Assays for Studying Quadruplex Ligands. *Methods* **2007**, *42*, 183−195.

(24) Monchaud, D.; Allain, C.; Teulade-Fichou, M. P. Development of a Fluorescent Intercalator Displacement Assay (G4-FID) for Establishing Quadruplex-DNA Affinity and Selectivity of Putative Ligands. *Bioorg. Med. Chem. Lett.* **2006**, *16*, 4842−4845.

(25) Zuffo, M.; Guédin, A.; Leriche, E.-D.; Doria, F.; Pirota, V.; Gabelica, V.; Mergny, J.-L.; Freccero, M. More Is Not Always Better: Finding the Right Trade-off between Affinity and Selectivity of a G-Quadruplex Ligand. *Nucleic Acids Res.* **2018**, *46*, No. e115.

(26) Jerabek-Willemsen, M.; Wienken, C. J.; Braun, D.; Baaske, P.; Duhr, S. Molecular Interaction Studies Using Microscale Thermophoresis. *Assay Drug Dev. Technol.* **2011**, *9*, 342−353.

(27) Nanni, P.; Landuzzi, L.; Nicoletti, G.; De Giovanni, C.; Giovarelli, M.; Lalli, E.; Facchini, A.; Lollini, P. L. Control of H-2 Expression in Transformed Nonhaemopoietic Cells by Autocrine Interferon. *Br. J. Cancer* **1992**, *66*, 479−482.

(28) Biffi, G.; Di Antonio, M.; Tannahill, D.; Balasubramanian, S. Visualization and Selective Chemical Targeting of RNA G-Quadruplex Structures in the Cytoplasm of Human Cells. *Nat. Chem.* **2014**, *6*, 75−80.

(29) Crowl, J. T.; Gray, E. E.; Pestal, K.; Volkman, H. E.; Stetson, D. B. Intracellular Nucleic Acid Detection in Autoimmunity. *Annu. Rev. Immunol.* **2017**, *35*, 313−336.

(30) Pilger, D.; Seymour, L. W.; Jackson, S. P. Interfaces between Cellular Responses to DNA Damage and Cancer Immunotherapy. *Genes Dev.* **2021**, *35*, 602−618.

(31) Beauvarlet, J.; Bensadoun, P.; Darbo, E.; Labrunie, G.; Rousseau, B.; Richard, E.; Draskovic, I.; Londono-Vallejo, A.; Dupuy, J.-W.; Nath Das, R.; Guédin, A.; Robert, G.; Orange, F.; Croce, S.; Valesco, V.; Soubeyran, P.; Ryan, K. M.; Mergny, J.-L.; Djavaheri-Mergny, M. Modulation of the ATM/Autophagy Pathway by a G-Quadruplex Ligand Tips the Balance between Senescence and Apoptosis in Cancer Cells. *Nucleic Acids Res.* **2019**, *47*, 2739−2756.

(32) Zhou, W. J.; Deng, R.; Zhang, X. Y.; Feng, G. K.; Gu, L. Q.; Zhu, X. F. G-Quadruplex Ligand SYUIQ-5 Induces Autophagy by Telomere Damage and TRF2 Delocalization in Cancer Cells. *Mol. Cancer Ther.* **2009**, *8*, 3203−3213.

(33) Gui, X.; Yang, H.; Li, T.; Tan, X.; Shi, P.; Li, M.; Du, F.; Chen, Z. J. Autophagy Induction via STING Trafficking Is a Primordial Function of the CGAS Pathway. *Nature* **2019**, *567*, 262−266.

(34) Hopfner, K.-P.; Hornung, V. Molecular Mechanisms and Cellular Functions of CGAS−STING Signalling. *Nat. Rev. Mol. Cell Biol.* **2020**, *21*, 501−521.

https://doi.org/10.1021/acs.jmedchem.2c00772
J. Med. Chem. 2022, 65, 12055−12067

(35) Amato, J.; Mashima, T.; Kamatari, Y. O.; Kuwata, K.; Novellino, E.; Randazzo, A.; Giancola, C.; Katahira, M.; Pagano, B. Improved Anti-Prion Nucleic Acid Aptamers by Incorporation of Chemical Modifications. *Nucleic Acid Ther.* **2020**, *30*, 414−421.
(36) Cantor, C. R.; Warshaw, M. M.; Shapiro, H. Oligonucleotide Interactions. III. Circular Dichroism Studies of the Conformation of Deoxyoligonucleolides. *Biopolymers* **1970**, *9*, 1059−1077.
(37) Amato, J.; Madanayake, T. W.; Iaccarino, N.; Novellino, E.; Randazzo, A.; Hurley, L. H.; Pagano, B. HMGB1 Binds to the KRAS Promoter G-Quadruplex: A New Player in Oncogene Transcriptional Regulation? *Chem. Commun.* **2018**, *54*, 9442−9445.

https://doi.org/10.1021/acs.jmedchem.2c00772
J. Med. Chem. 2022, 65, 12055−12067